JOURNAL OF PROPULSION AND POWER
Vol. 24, No. 3, May–June 2008

Ultrasonic Propulsion

Eric M. Allison,* George S. Springer,† and Jacques Van Dam‡
Stanford University, Stanford, California 94305

DOI: 10.2514/1.30044

A propulsion system is introduced for propelling and guiding an object through a liquid. Thrust for forward motion and for turning is produced by acoustic waves generated by piezoelectric ultrasonic transducers. The principle of operation of the transducers and methods for their design are described. Test results are presented that validate the concepts and the design methods and illustrate the fact that ultrasonic propulsion may be employed in situations where the use of conventional propulsion devices such as propellers and jets is unfeasible.

Nomenclature

A	=	wetted cross-sectional area of the capsule, m^2
a	=	radius of the transducer, m
C_0	=	zero-strain capacitance, F
c	=	acoustic wave speed, m/s
c_d	=	drag coefficient
c_p^s	=	stiffened acoustic wave speed in the piezoelectric resonator, m/s
D	=	diameter of the capsule, m
$\hat{F}'$	=	force per unit volume in the x' direction, N
f	=	frequency of transducer excitation, Hz
f_0	=	operating frequency, Hz
G	=	a point for control volume analysis in the far field
h	=	thickness, m
I'	=	far-field intensity in the x' direction, W/m^2
I'_0	=	intensity at the surface of the transducer, W/m^2
$I'_{0,\theta=0}$	=	intensity at the surface of the transducer along the x axis, W/m^2
i	=	electrical current through the transducer, A
J_1	=	Bessel function of the first type
j	=	imaginary number ($\sqrt{(-1)}$)
k	=	wave number, m^{-1}
P	=	total acoustic power emitted, W
P_{in}	=	incident power at an interface, W
P_{req}	=	acoustic power needed to generate the required thrust, W
P_{tran}	=	transmitted power at an interface, W
P_x	=	acoustic power propagated normal to the transducer face, W
P'	=	acoustic power in the x' direction, W
P^*	=	power ratio, $\frac{P_x}{P}$
p_0	=	parameter defined as $\rho c v_0$, N/m^2
$\mathcal{R}$	=	resistance, the real part of the electrical impedance of the transducer, Ω
Re	=	Reynolds number
R_0	=	Raleigh distance, m
r	=	spherical coordinate, the radial distance from the center of the transducer
S	=	surface area of a hemisphere surrounding the transducer, m^2
s	=	speed of the capsule, m/s
T	=	thrust, the force normal to the transducer face, N
T_{req}	=	required thrust for a specific application, N
t	=	time, s
u	=	fluctuating fluid velocity in the acoustic wave, m/s
V	=	total fluid volume, m^3
$\mathcal{V}$	=	voltage applied to the transducer, V
$\mathcal{V}_0$	=	amplitude of the voltage applied to the transducer, V
v_0	=	amplitude of the transducer face velocity, m/s
$\mathcal{X}$	=	reactance, the imaginary part of the electrical impedance of the transducer, Ω
x	=	coordinate axis perpendicular to the face of the transducer
x'	=	coordinate along a ray extending out from the center of the transducer
Z	=	characteristic acoustic impedance, Pa · s/m
$\tilde{Z}_L$	=	specific acoustic impedance to the left of an interface, $Pa \cdot s/m^3$
$\tilde{Z}_R$	=	specific acoustic impedance to the right of an interface, $Pa \cdot s/m^3$
$\mathcal{Z}^{\text{el}}$	=	electrical impedance of the transducer, Ω
β	=	proportional loss of acoustic energy per unit distance, m^{-1}
Γ_t	=	power transmission coefficient
η	=	overall transducer efficiency
η_p	=	efficiency to account for transducer model approximations
η_v	=	efficiency to account for losses in the transducer
θ	=	spherical coordinate, the angle between x' and x axes
κ_T	=	electromechanical coupling constant
λ	=	acoustic wavelength ($=\frac{c}{f}$), m
ν	=	kinematic viscosity of water, Pa · s
ρ	=	density, kg/m^3
ϕ	=	spherical coordinate, rotation about the x axis

Subscripts

b	=	transducer backing
f	=	fluid in front of transducer
ℓ	=	transducer matching layer
p	=	transducer piezoelectric resonator

Received 26 January 2007; accepted for publication 28 November 2007.

*Research Assistant, Department of Aeronautics and Astronautics. Student Member AIAA.

†Paul Pigott Professor of Engineering, Department of Aeronautics and Astronautics. Fellow AIAA.

‡Professor of Medicine, Stanford University School of Medicine.

I. Introduction

THE thrust required to move an object through a fluid is commonly produced by propellers or jets. This investigation describes a propulsion system that does not rely on either of these means of creating thrust. The system uses the force generated when a transducer broadcasts acoustic streams into the surrounding fluid (Fig. 1). The underlying concepts of this system are described in the next section. Validation tests are presented in Sec. III.

Streaming in a fluid caused by acoustic waves has been studied previously and is described in the excellent treatise by Lighthill [1,2] and in the comprehensive summary of Boluriaan and Morris [3].

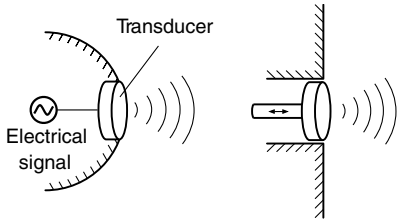

Fig. 1 Acoustic waves generated by a transducer mounted on a body and by a vibrating piston mounted in an infinite baffle.

Acoustic streaming has been suggested for pumping and mixing liquids, for manipulating objects immersed in a liquid, for forming and ejecting liquid droplets, for driving Helmholtz resonators used to provide micropropulsion in air, and for cooling integrated circuits. A survey of the related literature is given by Allison [4]. It seems that acoustic streams have not yet been used in practice to generate thrust, the topic that is the subject of the present work.

II. Propulsion System

The main objective of this investigation is to design an acoustic propulsion system that produces the thrust required for driving a body through a fluid. The thrust is generated by acoustic waves produced by a transducer that converts a sinusoidal electrical signal into mechanical vibrations (Fig. 1). The operation of the propulsion system is presented in this section. First, however, the means are described by which the thrust is generated.

A. Thrust and Power

When a transducer emits acoustic waves into a fluid a force is generated on the surface of the transducer. We are interested in the magnitude of this force (referred to as thrust) and the power required to generate it. In practice, the transducer is mounted on a finite body (Fig. 1). Here, we model the transducer configuration by a rigid, flat, circular piston of diameter $2a$ mounted in an infinite baffle surrounded by a semi-infinite fluid. The piston vibrates with simple harmonic motion producing an acoustic field in the fluid. The approximations introduced by this model and in the analyses that follow are accounted for at the end of this section.

The fluid partially absorbs the acoustic waves, resulting in a decrease in the mean momentum flux as the waves travel through the fluid. A net force is associated with this decrease in the momentum flux. To calculate this net force, we consider a control volume of length $\mathrm{d}x'$ at point G in the far field (Fraunhofer diffraction) region [5] (Fig. 2). Locally, we treat the waves as plane, traveling in the longitudinal x' direction of the control volume. The difference between the leaving and entering momentum fluxes is $(\partial\overline{\rho u^2}/\partial x')\,\mathrm{d}x'$ [1], where the bar represents time average at a point. The law of conservation of momentum for a control volume of slowly varying cross section reduces to that of a control volume of constant cross section [6]. Thus, conservation of momentum for the control volume at point G (Fig. 2) gives the force in the radial x' direction[1]

$$\hat{F}' = -\frac{\partial\overline{\rho u^2}}{\partial x'} \tag{1}$$

This equation may be rewritten in terms of the far-field intensity I' (power per unit area) [1]

$$\hat{F}' = \frac{\beta}{c} I' \tag{2}$$

In the near-field region (Fig. 2), which extends to a distance of about $0.75a^2/\lambda$ from the piston [5], the acoustic field is characterized by interference phenomena. Because of the complex nature of these phenomena, following Lighthill we calculate the thrust by extending the far-field expression for the intensity up to the face of the piston. The resulting analysis is not limited to any wavelength, and for the geometries tested yielded good results (see Sec. III). With this approximation, at a radial distance r from the center of the piston, the intensity is [1]

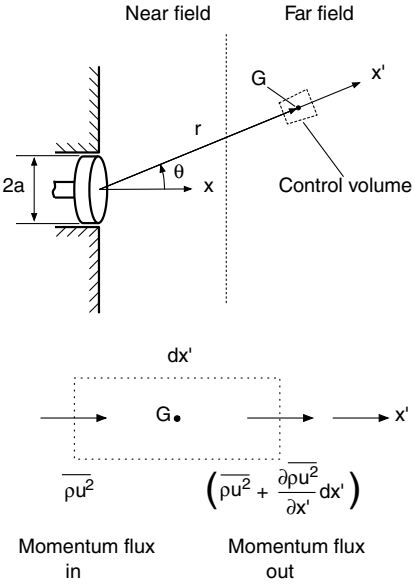

Fig. 2 The near field and far field and the control volume at point G (top) and the mean momentum flux into and out of the control volume (bottom).

$$I' = I'_0 e^{-\beta r} \tag{3}$$

I'_0 is the value of the intensity at the surface of the piston ($r = 0$) [7]

$$I'_0 = I'_{0,\theta=0}\left[\frac{2J_1(ka\sin\theta)}{ka\sin\theta}\right]^2 \tag{4}$$

where k is the wave number

$$k = \frac{2\pi f}{c} \tag{5}$$

$I'_{0,\theta=0}$ is the value of I'_0 along the x axis ($\theta = 0$) [6]

$$I'_{0,\theta=0} = \frac{p_0^2 R_0^2}{2\rho c r^2} \tag{6}$$

where R_0 ($=ka^2/2$) is the Raleigh distance, and p_0 is a parameter defined as $p_0 = \rho c v_0$. Equations (3), (4), and (6) yield

$$I' = \frac{p_0^2 R_0^2}{2\rho c r^2}\left[\frac{2J_1(ka\sin\theta)}{ka\sin\theta}\right]^2 e^{-\beta r} \tag{7}$$

The thrust T is the force normal to the face of the piston generated by forces $\hat{F}'$ inside the entire fluid

$$T = \int_V \hat{F}'\cos\theta\,\mathrm{d}V \tag{8}$$

The volume element $\mathrm{d}V$ is shown in Fig. 3. By applying spherical coordinates, we obtain [Eqs. (2) and (8)]

$$T = \int_0^\infty \int_0^{2\pi} \int_0^{\frac{\pi}{2}} \frac{\beta}{c} I' \cos\theta \sin\theta r^2\,\mathrm{d}\theta\,\mathrm{d}\phi\,\mathrm{d}r \tag{9}$$

Equations (7) and (9) yield the following expression for the thrust:

$$T = \frac{1}{c}\left[\frac{p_0 v_0 R_0^2}{(ka)^2} 4\pi \int_0^{\frac{\pi}{2}} \frac{J_1(ka\sin\theta)^2\cos\theta}{\sin\theta}\,\mathrm{d}\theta\right] \tag{10}$$

The acoustic power propagating in the x' direction and passing through an area $\mathrm{d}S$ (Fig. 3) is [2]

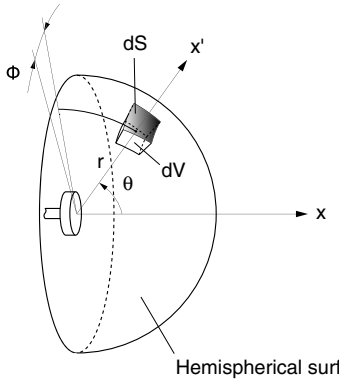

Fig. 3 The volume element used in Eqs. (9) and (10) for calculating the thrust.

$$P' = I'\,\mathrm{d}S \tag{11}$$

The acoustic power P_x propagating in the direction normal to the piston face is

$$P_x = \int_S I' \cos\theta\,\mathrm{d}S = \int_S I'_0 \cos\theta\,\mathrm{d}S e^{-\beta r} \tag{12}$$

where the second expression is written by the use of Eq. (3). We are interested in the initial power P_x^0 which is the power at $r = 0$. Setting $r = 0$ and substituting Eq. (7) into Eq. (12) gives

$$P_x^0 = \frac{p_0 v_0 R_0^2}{(ka)^2} 4\pi \int_0^{\frac{\pi}{2}} \frac{J_1(ka\sin\theta)^2 \cos\theta}{\sin\theta}\,\mathrm{d}\theta \tag{13}$$

Equations (10) and (13) provide the relationship between P_x^0 and the thrust T

$$P_x^0 = cT \tag{14}$$

The total acoustic power emitted is [6]

$$P = \frac{\pi a^2}{2\rho c} p_0^2 \left[1 - \frac{2J_1(2ka)}{2ka}\right] \tag{15}$$

Maximum thrust is generated when all the acoustic power is propagating normal to the surface of the piston ($P_x^0 = P$). We introduce the power ratio P^*

$$P^* = \frac{P_x^0}{P} = 2\left[\int_0^{\frac{\pi}{2}} \frac{J_1(ka\sin\theta)^2 \cos\theta}{\sin\theta}\,\mathrm{d}\theta\right] \Big/ \left[1 - \frac{2J_1(2ka)}{2ka}\right] \tag{16}$$

For a given application the thrust required T_{req} is specified. Equations (14) and (16) give the acoustic power needed to generate this required thrust

$$P_{\mathrm{req}} = \frac{T_{\mathrm{req}} c}{P^*} \tag{17}$$

In this model, we assume that $(P - P_x^0)$ produces symmetric forces that do not contribute to the thrust. This power may also contribute to near-field effects not modeled in this treatment.

In the aforementioned analyses we introduced three important approximations, namely, that the fluid is semi-infinite, the face of the transducer moves uniformly as would the face of a rigid piston, and the forces in the near field can be represented by the far-field forces. We take into account these approximations by introducing an efficiency η_p, and express the required acoustic power as

$$P_{\mathrm{req}} = \frac{T_{\mathrm{req}} c}{P^* \eta_p} \tag{18}$$

We calculated the power ratio P^* by Eq. (16) and present the results in Fig. 4 for transducers vibrating at different frequencies. The results in Fig. 4 show that regardless of the transducer diameter the power ratio rapidly increases with increasing frequency. Thus, at high frequencies (where $P^* \approx 1$) the required acoustic power may be approximated by

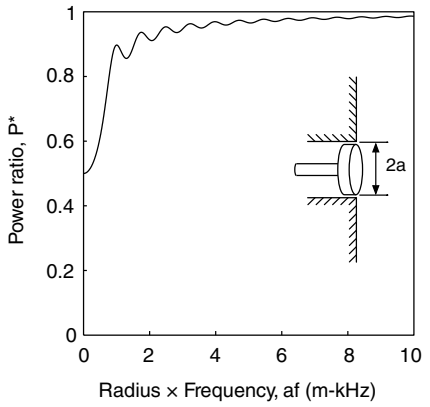

Fig. 4 The power ratio versus the parameter *af*.

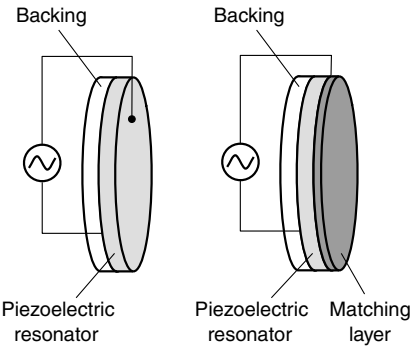

Fig. 5 Transducer without and with matching layer.

$$P_{\mathrm{req}} \approx \frac{T_{\mathrm{req}} c}{\eta_p} \tag{19}$$

B. Transducer

The main element of the transducer is a resonator that transforms sinusoidal electrical signals into harmonic vibrations. These vibrations are transmitted into the surrounding fluid in the form of acoustic waves. Different types of resonators may be used to produce acoustic waves. Here, we consider tranducers that use a piezoelectric material as the resonator. On one side of the resonator is a backing material. The other side may either be exposed directly to a fluid or to a layer (referred to as the matching layer) placed between the resonator and the fluid (Fig. 5). The thicknesses of the piezoelectric resonator, the backing, and the matching layer are h_p, h_b, and h_ℓ, respectively (Fig. 6). The fluid is taken to be semi-infinite.

The characteristic (acoustic) impedances of the piezoelectric material, the backing, the matching layer, and the fluid are defined as [8]

$$Z_p = \rho_p c_p^s \qquad Z_b = \rho_b c_b \qquad Z_\ell = \rho_\ell c_\ell \qquad Z_f = \rho_f c_f \tag{20}$$

We need to select the thicknesses and the materials of the components of the transducer such that the electrical input power is transmitted efficiently to the fluid. For maximum efficiency the resonator should operate near its natural frequency f_0, to ensure that right- and left-traveling waves reinforce each other. A transducer transmitting into a fluid operates at its natural frequency when the thickness of the resonator is either $h_p = \lambda_p/2$ (when $Z_b \ll Z_p$) or $h_p = \lambda_p/4$ (when $Z_b \gg Z_p$) [8].

For maximum power transmission into the fluid, a backing with a characteristic impedance lower than that of the piezoelectric material is needed. In this case the thickness is

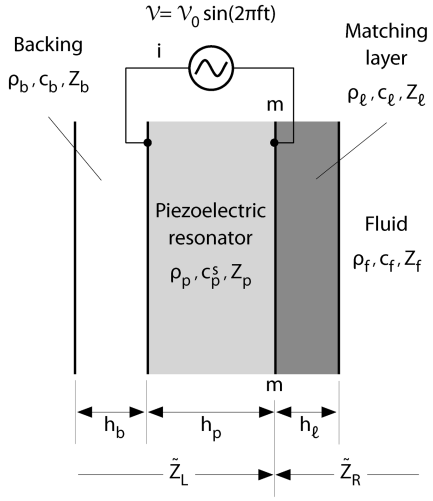

Fig. 6 Transducer with specific acoustic impedances $\tilde{Z}_R$ and $\tilde{Z}_L$ to the right and to the left of the *m-m* interface and exposed to a semi-infinite fluid.

$$h_p = \frac{\lambda_p}{2} \qquad (Z_b \ll Z_p) \tag{21}$$

where the wavelength is $\lambda_p = c_p^s/f_0$. The natural frequency f_0 is a design parameter and is chosen so as to satisfy the requirement that the power ratio P^* is close to unity (Sec. II.A).

For example, air is a suitable backing material for a high-efficiency piezoelectric transducer because its characteristic impedance ($Z_{\text{air}} \approx 400$ Pa · s/m) is small compared to the characteristic impedance of typical piezoelectric materials ($Z_p \approx 35$ MPa · s/m). Equation (21) does not place any restriction on the thickness of the backing. Once the condition $Z_b \ll Z_p$ is satisfied, wave transfer into the backing is negligible, and the thickness of the backing is irrelevant.

The thickness of the matching layer (if one is applied) is established by the requirement that the acoustic waves traveling through the matching layer reinforce each other. This requirement is met when the matching layer's thickness is [9]

$$h_\ell = \frac{\lambda_\ell}{4} \tag{22}$$

where λ_ℓ is the wavelength in the matching layer ($\lambda_\ell = c_\ell/f_0$).

Equations (21) and (22) provide the thicknesses of the resonator and the matching layer and the type of material (i.e., the required value of Z_b) for the backing. It remains to determine the material properties of the matching layer. To this end, we introduce the power transmission coefficient defined as [8]

$$\Gamma_t = \frac{P_{\text{tran}}}{P_{\text{in}}} \tag{23}$$

where P_{in} and P_{tran} are the incident and transmitted powers at an interface. For waves traveling from left to right the power transmission coefficient may be expressed in terms of the specific (acoustic) impedances $\tilde{Z}_L$ and $\tilde{Z}_R$ (defined as the ratio of acoustic pressure to velocity) of the materials to the left and to the right of the interface (Fig. 6). In terms of $\tilde{Z}_L$ and $\tilde{Z}_R$ the transmission coefficient is [8]

$$\Gamma_t = 1 - \left(\frac{\tilde{Z}_R - \tilde{Z}_L}{\tilde{Z}_R + \tilde{Z}_L}\right)^2 \tag{24}$$

When the transmission coefficient is unity ($\Gamma_t = 1$), all the power is transmitted across the interface. This condition is met when $\tilde{Z}_L$ equals $\tilde{Z}_R$.

We treat the piezoelectric material as linearly elastic and, inside the transducer, we consider the waves to be plane traveling normal to the surface. The latter approximation is reasonable when the cross-sectional dimensions of the transducer are large compared to the wavelength inside the resonator [8]. Then, the specific impedance to the right of interface *m-m*, shown in Fig. 6, is [8]

$$\tilde{Z}_R = \begin{cases} Z_f & \text{no matching layer} \\ Z_\ell \frac{Z_f \cos k_\ell h_\ell + jZ_\ell \sin k_\ell h_\ell}{Z_\ell \cos k_\ell h_\ell + jZ_f \sin k_\ell h_\ell} & \text{with matching layer} \end{cases} \tag{25}$$

When the backing is opaque ($Z_b = 0$), the specific impedance to the left of the interface is obtained by rearranging the expressions given by Kino [8]. The result is

$$\tilde{Z}_L = \frac{jZ_p[2\kappa_T^2(\cos k_p h_p - 1)]}{\kappa_T^2 \sin k_p h_p + k_p h_p \cos k_p h_p (j2\pi f C_0 \mathcal{Z}^{\text{el}} - 1)} + \frac{jZ_p k_p h_p \sin k_p h_p (1 - j2\pi f C_0 \mathcal{Z}^{\text{el}})}{\kappa_T^2 \sin k_p h_p + k_p h_p \cos k_p h_p (j2\pi f C_0 \mathcal{Z}^{\text{el}} - 1)} \tag{26}$$

where $\mathcal{Z}^{\text{el}}$ is the electrical impedance defined as the ratio of the voltage $\mathcal{V}$ to the current i. To ensure that the *m-m* interface is transparent to the acoustic waves traveling from the resonator into the fluid, we equate $\tilde{Z}_R$ and $\tilde{Z}_L$. Equation (26), together with $\tilde{Z}_L = \tilde{Z}_R$, gives

$$\mathcal{Z}^{\text{el}} = \frac{1}{j2\pi f C_0} + \frac{\kappa_T^2[j\tilde{Z}_R \sin k_p h_p - 2Z_p(1 - \cos k_p h_p)]}{j2\pi f C_0 (Z_p \sin k_p h_p - j\tilde{Z}_R \cos k_p h_p) k_p h_p} \tag{27}$$

where $\tilde{Z}_R$ is given by Eq. (25). Note that the electrical impedance depends on the frequency through k_p and k_ℓ.

We use Eq. (27) to determine the most suitable material (as specified by the characteristic impedance Z_ℓ) for the matching layer. As a first step, we calculate the real part $\mathcal{R}$ of the electrical impedance (referred to as the resistance) of an air-backed transducer transmitting into water. The results are presented in Fig. 7 and include the natural frequency of the resonator ($f_0 = c_p^s/h_p = 5$ MHz), the frequency at which the resonator operates most efficiently. From Fig. 7 [which is a representation of Eq. (27)] it is seen that the natural frequency f_0 is close to the frequency at which the resistance is maximum [9]. This implies that the transducer should operate at the maximum electrical resistance.

Without the matching layer the resistance has a very sharp peak at f_0 and falls off rapidly with increasing and decreasing frequencies. This is undesirable because, in practice, it is very difficult to set the frequency precisely at the desired value corresponding to the peak. The consequence of this is that if the operating frequency differs even slightly from the natural frequency, the system operates at an electrical impedance $\mathcal{Z}^{\text{el}}$ that differs from that for which the system was designed. As a result, the *m-m* interface is not transparent to the acoustic waves traveling from the resonator into the fluid.

The aforementioned shortcoming may be overcome by the addition of a matching layer having a properly chosen characteristic impedance Z_ℓ. Desilets and his coworkers have shown that the value of the resistance varies only slightly over a range of frequencies about

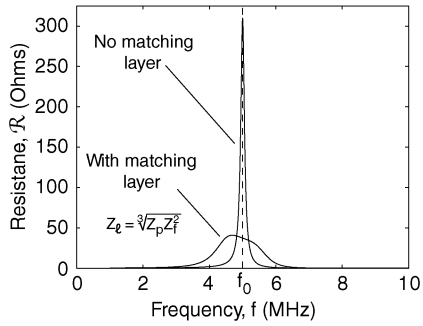

Fig. 7 Resistance of a transducer with and without a matching layer, where f_0 is the natural frequency of the resonator. Values used for the calculation are in Table 1.

f_0 when the characteristic impedance of the matching layer is [9]

$$Z_\ell = \sqrt[3]{Z_p Z_f^2} \tag{28}$$

For a transducer with a matching layer having the characteristic impedance specified by Eq. (28), the $\mathcal{R}$ versus frequency curve is "flatter" than for a transducer without a matching layer (Fig. 7).

The frequency range over which the electrical impedance is flat may be extended by additional matching layers [9]. In the present application an adequate frequency range is achieved with only one matching layer. Therefore, additional matching layers are unnecessary; they are also undesirable as additional layers would increase internal losses.

When the real part (resistance $\mathcal{R}$) of the transducer's electrical impedance is large compared to the imaginary part (reactance $\mathcal{X}$), the voltage required to power the transducer is calculated as follows. For a sinusoidal applied voltage ($\mathcal{V} = \mathcal{V}_0 \sin 2\pi f_0 t$), the amplitude of the input voltage is [10]

$$\mathcal{V}_0 = \sqrt{2P_{\text{req}}\mathcal{R}} \tag{29}$$

where P_{req} is the required power given by Eq. (19).

The aforementioned analyses do not take into account losses inside the transducer. Even when the thicknesses and the material properties are selected as described above, due to internal losses not all of the electrical power input into the transducer is transmitted into the fluid. These losses are accounted for by an efficiency η_v. By applying this efficiency to Eq. (19), the required electrical power input is

$$P_{\text{req}} = \frac{T_{\text{req}} c_f}{\eta_p \eta_v} = \frac{T_{\text{req}} c_f}{\eta} \tag{30}$$

III. Validation Tests

We performed two types of tests to assess the validity and practical viability of the concepts described in the previous sections. In the first type of test we measured the performance of the transducer; in the second we assessed the operation of a system designed to propel and wirelessly guide a capsule through water.

A. Transducer Performance

We built a transducer consisting of four main components: the resonator, matching layer, backing, and housing (Figs. 6 and 8).

The resonator is a 10-mm diam and 0.43-mm thick disk made of lead zirconate titanate (PZT), a piezoelectric material (Table 2) with aluminum electrodes deposited on each side. The operating frequency corresponding to this thickness is

$$f_0 = c_p^s / 2h_p = \frac{4680}{2 \times 0.00043} = 5.5 \text{ MHz}$$

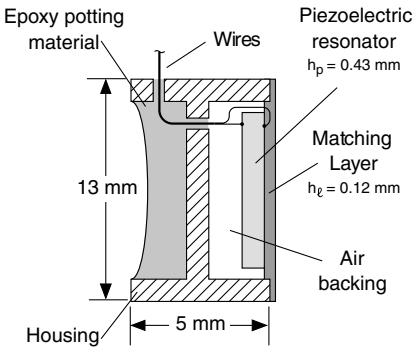

Fig. 8 The transducer used in the proof-of-concept capsule. Material properties are given in Table 2.

Table 1 The properties used in calculating the results in Fig. 7

Property	Value
Zero-strain capacitance, C_0, nF	1.03
Wave speed in the matching layer, c_ℓ, m/s	2000
Stiffened wave speed in the piezoelectric resonator, c_p^s, m/s	4670
Thickness of the matching layer, h_ℓ, mm	0.1
Thickness of the piezoelectric resonator, h_p, mm	0.467
Characteristic impedance of the backing, Z_b, (Pa · s)/m	0
Characteristic impedance of the fluid (water), Z_f, (MPa · s)/m	1.48
Characteristic impedance of the matching layer, Z_ℓ, (MPa · s)/m	4.27
Characteristic impedance of the piezoelectric resonator, Z_p, (MPa · s)/m	35.5
Electromechanical coupling constant, κ_T	0.57

Table 2 Properties of the piezoelectric material in the proof-of-concept transducer

Manufacturer specified[a]	
Relative dielectric constant	$K_{33}^T = 1284$
Electromechanical coupling factor	$k_p = 0.60$, $k_{33} = 0.68$, $k_{31} = 0.33$
	$k_{15} = 0.67$, $k_t\ (=\kappa_T) = 0.46$
Piezoelectric charge constant, 10^{-12} C/N	$d_{33} = 300$, $d_{31} = -109$, $d_{15} = 450$
Piezoelectric voltage constant, 10^{-3} (V · m)/N	$g_{33} = 25.5$, $g_{31} = -10.5$, $g_{15} = 35$
Young's modulus, 10^{10} N/m^2	$Y_{11}^E = 7.6$, $Y_{33}^E = 6.3$
Frequency constants, m/s	$N_L = 1700$, $N_T = 2005$, $N_P = 2055$
Density, kg/m^3	$\rho_p = 7600$
Calculated[b]	
Zero-strain capacitance	$C_0 = 1.66$ nF
Stiffened wave speed	$c_p^s = 4680$ m/s
Characteristic impedance	$Z_p = 35.5$ (MPa · s)/m

[a]APC, Inc. (http://www.americanpiezo.com), material APC841.
[b]Reference [4].

The matching layer is a 10-mm diam disk made of epoxy cast in place over the resonator ($\rho_\ell = 1160$ kg/m^3, $c_\ell = 2620$ m/s). The thickness corresponding to the 5.5 MHz frequency is

$$h_\ell = \frac{2620}{(4)(5.5 \times 10^6)} = 0.12 \text{ mm}$$

[see Eq. (22)]. The actual thickness is 0.17 mm. The matching layer's characteristic impedance calculated by Eq. (20) is $Z_\ell = 3.04$ MPa · s/m while the desired value given by Eq. (28) is $Z_\ell = 4.27$ MPa · s/m. For the present application the differences between the calculated and actual thicknesses and between the calculated and actual characteristic impedances were deemed acceptable. A transducer with the calculated values of the thickness and the impedance would have provided a more flat resistance vs frequency response than the actual transducer that was built. This would have made it easier to set the amplifier providing power to the transducer at the desired frequency. However, even as built it was possible to tune the amplifier to the correct frequency.

The resonator–matching layer unit is enclosed in a plastic housing. A 1.5-mm air gap is between the resonator and the housing, serving as the backing ($Z_b \approx 0$). The electrical wires are attached to the resonator by conductive epoxy.

Four identical transducers of the dimensions shown in Fig. 8 were fabricated. The electrical impedances of all four transducers were measured by a Hewlett-Packard 8505A network analyzer. The electrical impedances were also calculated by Eq. (27) using the parameters listed in Table 2 and described previously. The measured and calculated impedances are presented in Fig. 9. We note that at the

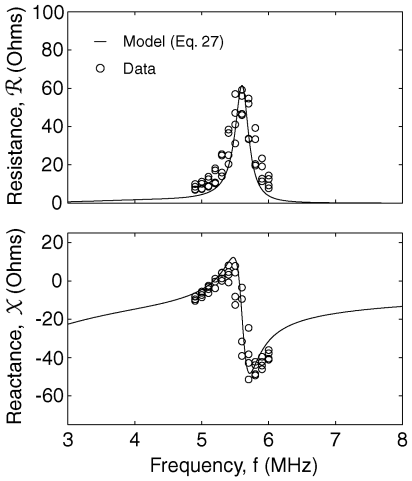

Fig. 9 The real $\mathcal{R}$ and imaginary $\mathcal{X}$ parts of the electrical impedance of the transducer shown in Fig. 8.

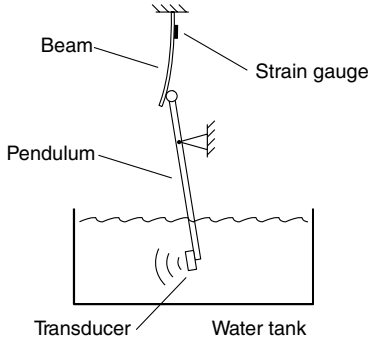

Fig. 10 Schematic of the test setup for measuring transducer efficiency.

operating frequency of 5.5 MHz both the calculated and measured resistances are near 60 Ω.

The thrust produced and the efficiency were measured by a device consisting of a 300-mm long, carefully balanced pendulum and a beam instrumented by a strain gauge (Fig. 10). The transducer was fitted on one end of the pendulum. The other end of the pendulum was in contact with the beam. The transducer was placed in a water tank and was activated by a signal generator. The thrust developed by the transducer was deduced from the calibrated output of the strain gauge. The power input to the transducer was calculated by the expression $P = \mathcal{V}_0^2/2\mathcal{R}$ [Eq. (29)]. $\mathcal{V}_0$ was measured by an oscilloscope, and $\mathcal{R}$ is the measured value of the transducer resistance. The power versus thrust data and the relationship $P = \frac{T \cdot c_f}{\eta}$ [Eq. (30)] are given in Fig. 11. The data show a linear relationship between the power and the thrust and bear out Eq. (30).

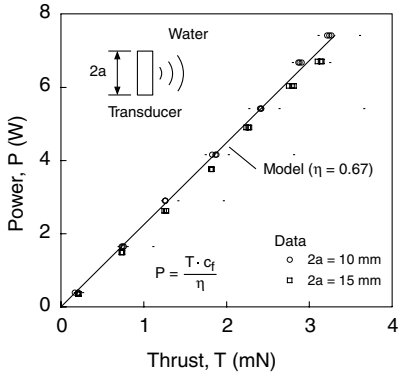

Fig. 11 Power versus thrust in water ($c_f = 1480$ m/s, $\eta = 0.67$).

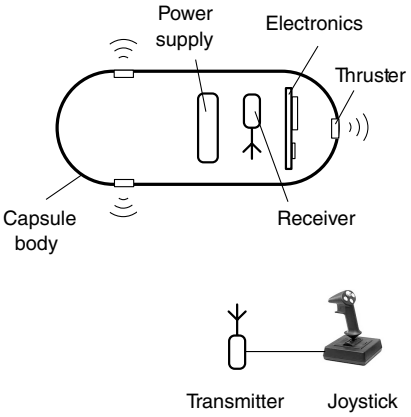

Fig. 12 Schematic of the proof-of-concept device.

B. Proof-of-Concept System

A proof-of-concept system was built consisting of a capsule and an external guidance system (Fig. 12).

The capsule body is made of three 50-mm outside diam, 1.27-mm thick cylindrical segments (Fig. 13). One of the segments is 25 mm long; the other two are 65 mm long. The two long segments are attached to the short one by watertight, frictional connections. Each end of the capsule is capped by a transparent hemispherical dome. There is a 13-mm diam hole in the aft dome to accommodate the transducer used for providing the primary thrust. There are two 13-mm diam holes on opposite sides in the forward cylindrical segment for the transducers that provide thrust for steering. The capsule was weighted in such a manner so as to minimize rolling, thereby ensuring maximum effectiveness of the side thrusters. A photograph of the capsule is shown in Fig. 14.

For a desired capsule speed of $s = 85$ mm/s the Reynolds number is $Re = 4100$. The corresponding drag coefficient is $c_d = 0.4$. For a capsule floating in water at a depth of $y = 0.75D$, the wetted area is $A = 1630$ mm^2 and the force is 2.25 mN. The power required to generate this thrust is [Eq. (30)]

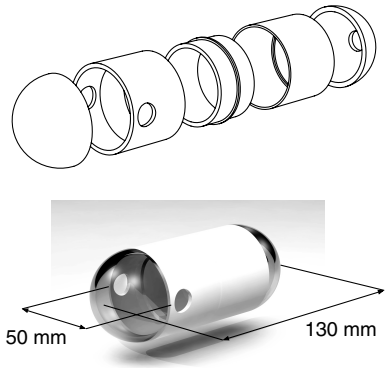

Fig. 13 The capsule body.

Fig. 14 The proof-of-concept capsule.

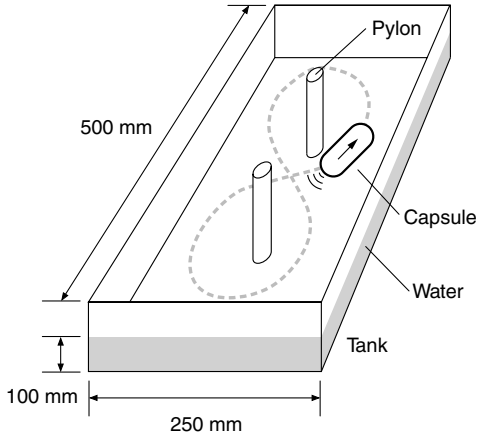

Fig. 15 The capsule on the surface of 22°C water guided wirelessly in a figure-eight pattern around two pylons.

$$P_{\text{req}} = \frac{T_{\text{req}} c_f}{\eta} = 5.0 \text{ W} \tag{31}$$

The resistance ($\mathcal{R} = 60\ \Omega$) is large compared to the reactance (Fig. 9), and the required amplitude of the sinusoidal voltage input is [Eq. (29)]

$$\mathcal{V}_0 = \sqrt{2P_{\text{req}}\mathcal{R}} = 24.5 \text{ V} \tag{32}$$

Details of the electrical circuits are given by Allison [4].

The proof-of-concept system was tested by placing the capsule in a water tank. The capsule was then guided wirelessly to demonstrate the viability of the propulsion and guidance systems. When traveling in a straight line the speed of the capsule was 75 mm/s. This compares favorably with the speed of 85 mm/s for which the capsule was designed. Maneuverability was demonstrated by navigating the capsule in a figure-eight pattern around two pylons placed 150 mm apart (Fig. 15).

IV. Conclusions

The ultrasonic propulsion system developed during the course of this investigation provides a practical means to propel and guide an object immersed in a fluid when it is infeasible to use propellers or jets. For example, an important application of the ultrasonic propulsion system would be in a small capsule for examining the lining of the stomach. Such a capsule could replace the currently accepted procedure which entails the insertion by a trained physician of an endoscope into the stomach of a sedated patient. The capsule would simplify the procedure on Earth and would make endoscopy feasible in situations such as in space, where a conventional examination would be impractical.

When using such a capsule endoscope, a patient would first ingest water and then swallow the capsule. The device, equipped with remotely controlled ultrasonic propulsion and guidance systems such as proposed in this paper, would be able to navigate through the ingested water in the patient's stomach. The capsule could also contain an optical system wirelessly transmitting real-time stereoscopic video images to a computer display [11]. The physician would use these images to guide the capsule and, importantly, to obtain detailed information on the lining of the stomach for diagnostic purposes. It is estimated [4] that a lithium battery would provide sufficient power for 40 min of operation of the capsule, and this is more than required for the examination.

Acknowledgments

This work was supported by the Bio-X Interdisciplinary Initiatives Program, Stanford University. The authors wish to thank G. S. Kino and B. T. Khuri-Yakub for their suggestions regarding the transducer analysis and J. Ellis for his help with the signal generator design. The authors are grateful to Zs. Király for his useful comments in building the proof-of-concept system.

References

[1] Lighthill, M. J., *Waves in Fluids*, Cambridge Univ. Press, Cambridge, England, U.K., 1978.

[2] Lighthill, M. J., "Acoustic Streaming," *Journal of Sound and Vibration*, Vol. 61, No. 3, 1978, pp. 391–418. doi:10.1016/0022-460X(78)90388-7

[3] Boluriaan, S., and Morris, P. J., "Acoustic Streaming: From Rayleigh to Today," *International Journal of Aeroacoustics*, Vol. 2, Nos. 3–4, 2003, pp. 255–292. doi:10.1260/147547203322986142

[4] Allison, E., "Ultrasonic Propulsion," Ph.D. Thesis, Stanford University, Stanford, CA, 2006.

[5] Zemanek, J., "Beam Behavior Within the Nearfield of a Vibrating Plate," *Journal of the Acoustical Society of America*, Vol. 49, No. 1, 1971, pp. 181–191. doi:10.1121/1.1912316

[6] Blackstock, D. T., *Fundamentals of Physical Acoustics*, Wiley, New York, 2000.

[7] Pierce, A. D., *Acoustics: An Introduction to its Physical Principles and Applications*, Acoustical Society of America, Melville, NY, 1989, p. 227.

[8] Kino, G. S., *Acoustic Waves: Devices, Imaging, and Analog Signal Processing*, Prentice–Hall, Englewood Cliffs, NJ, 1987.

[9] Desilets, C. S., Fraser, J. D., and Kino, G. S., "The Design of Efficient Broad-Band Piezoelectric Transducers," *IEEE Transactions on Sonics and Ultrasonics*, Vol. SU-25, No. 3, 1978, pp. 115–125.

[10] Nilsson, J., and Riedel, S., *Electric Circuits*, Pearson/Prentice–Hall, Upper Saddle River, NJ, 2005, pp. 383–458.

[11] Király, Z., Springer, G. S., and Van Dam, J., "Stereoscopic Vision System," *Optical Engineering*, Vol. 45, No. 4, 2006, p. 043006. doi:10.1117/1.2189856

C. Tan
Associate Editor